Sensitivity of the Inner-Shelf Circulation to the Form of the Eddy Viscosity Profile*

STEVEN J. LENTZ

Woods Hole Oceanographic Institution, Woods Hole, Massachusetts

(Manuscript received 12 April 1993, in final form 12 October 1993)

ABSTRACT

The sensitivity of the inner-shelf circulation to the form of the vertical mixing is examined using a steady, linear, two-dimensional, eddy viscosity model. For both alongshelf wind stress and pressure gradient forcing, the alongshelf circulation over the inner shelf is insensitive to the form of the eddy viscosity profile. However, the cross-shelf circulation is sensitive to the form of the eddy viscosity profile. In particular, the location and width of the cross-shelf divergence in the Ekman transport over the inner shelf, and hence the corresponding upwelling or downwelling, depend on the form of the eddy viscosity profile.

1. Introduction

Over the middle to outer continental shelf, the surface and bottom boundary layers are typically thin compared to the water depth (Lentz 1992; Lentz and Trowbridge 1991). Ekman (1905) pointed out that in this case the stress-driven transport within the boundary layers (Ekman transport) is perpendicular to the applied stress due to the earth's rotation. In shallow water the earth's rotation is less important; there is a direct transfer of the stress through the water column and the stress-driven transport is in the direction of the applied stress. Between these two extremes there must be a transition region characterized by a cross-shelf divergence in the Ekman transport due to the interaction of the surface and bottom boundary layers. The inner shelf is defined here to be this transition region. This definition differs from many of the previous uses of the term inner shelf (e.g., Allen et al. 1983), but is similar to the "nearshore region" defined by Mitchum and Clarke (1986). The inner shelf plays a key role in the overall shelf dynamics because it is the region where the shelf circulation adjusts to the presence of the coastal boundary condition. For example, in the simplest cases it is the cross-shelf divergence of the Ekman transport over the inner shelf that drives both coastal upwelling and wind-driven coastal-trapped waves (Gill and Clarke 1974).

The few attempts to model inner-shelf circulation have generally relied on simple eddy viscosity models. In his seminal paper, Ekman (1905) used a constant eddy viscosity to examine wind-driven, two-dimensional shelf circulation. His results indicate that the divergence in the Ekman transport occurs in water depths between about $4\delta_E$ and δ_E (Fig. 1), where $\delta_E = (2A_v/f)^{1/2}$ is the Ekman layer depth scale, A_v is a constant eddy viscosity, and f is the Coriolis parameter. Mitchum and Clarke (1986) used the constant eddy viscosity solution and the long-wave assumption to determine a coastal boundary condition for coastal-trapped wave theory.

There have been a number of model studies of the inner shelf based on eddy viscosity profiles that are linear near one or both boundaries (surface and bottom) (Thomas 1975; Witten and Thomas 1976; Jenter and Madsen 1989; Poon and Madsen 1991). This choice is motivated by observations that the velocity profile is logarithmic near the bottom (e.g., Weatherly 1972; Grant and Madsen 1986) and that a logarithmic region may exist near the surface (Richman et al. 1987; Lentz 1992; Agrawal et al. 1992). A logarithmic velocity profile and a constant stress region near the boundary are consistent with an eddy viscosity profile of the form $\kappa u_* z'$ near the boundary, where $\kappa = 0.4$ is von Kármán's constant, z' is vertical distance from the boundary, and $u_* = (\tau/\rho_0)^{1/2}$ is the shear velocity, with τ the stress at the boundary and ρ_0 a reference density (e.g., Thomas 1975). While observations suggest a linear eddy viscosity profile is a reasonable representation of the turbulent mixing near the boundaries, it is less clear what the appropriate form of the turbulent mixing should be in the interior of the water column, even for an unstratified flow. Commonly used eddy viscosity profiles can have very different interior eddy viscosities (e.g., Smith and Long 1976; Jenter and Madsen 1989; Signell et al. 1990). An obvious question is to what extent results are sensitive to the form of the eddy viscosity profile that is used in a model.

* WHOI Contribution Number 8331.

Corresponding author address: Dr. Steven J. Lentz, Woods Hole Oceanographic Institution, Woods Hole, MA 02543.
E-mail: slentz@whoi.edu

The objective of this study is to determine whether the inner-shelf circulation is sensitive to the form of the turbulent mixing profile. The focus is on subinertial motions and the cross-shelf divergence in the Ekman transport over the inner shelf. The turbulent mixing is parameterized in terms of various simple eddy viscosity profiles. Simple eddy viscosity profiles such as those cited below and the ones examined in this study neglect the influence of stratification. The most obvious motivation for using such models is their relative simplicity. Furthermore, simple eddy viscosity models may be a reasonable representation of the mixing over the relatively shallow inner shelf, where stratification may be weak or nonexistent (e.g., Lee et al. 1989; Lentz 1994). The goal is not to identify a particular form for the eddy viscosity profile as correct or even to suggest that a simple eddy viscosity is the best representation of turbulent mixing, but rather to determine whether certain aspects of the inner-shelf circulation are sensitive to variations in the form of the eddy viscosity profile.

This study uses a steady, linear, unstratified, two-dimensional model to investigate the sensitivity of the flow characteristics over the inner shelf to the form of the eddy viscosity profile. Descriptions of the model, the numerical scheme, and the different eddy viscosity profiles considered are given in section 2. In section 3 the characteristics of the flow field over the inner shelf for various forms of the eddy viscosity profile are compared. Two general cases are considered, flows driven by an alongshelf wind stress (section 3a) and by an alongshelf pressure gradient (section 3b). Results are discussed and summarized in section 4.

2. The model

a. Equations

A steady, linear, unstratified, two-dimensional model is used to focus on the sensitivity of the inner-shelf circulation to the form of the eddy viscosity profile. A right-handed coordinate system is adopted (Fig. 1) in which x is the cross-shelf coordinate, positive onshore; y is the alongshelf coordinate, positive poleward; and z is the vertical coordinate, positive upward. The momentum equation is

$$f\mathbf{k} \times \mathbf{v} = -\frac{1}{\rho_0}\nabla P + \frac{\partial}{\partial z}\left(A_v \frac{\partial \mathbf{v}}{\partial z}\right), \qquad (1)$$

where $\mathbf{v}(x, z)$ is the current vector, P is the pressure, and $A_v(x, z)$ is the eddy viscosity. The boundary conditions are

$$A_v \frac{\partial \mathbf{v}}{\partial z} = \frac{\boldsymbol{\tau}^S}{\rho_0} \quad \text{at} \quad z = z_{0S}, \qquad (2)$$

$$\mathbf{v} = 0 \quad \text{at} \quad z = -D + z_{0B}, \qquad (3)$$

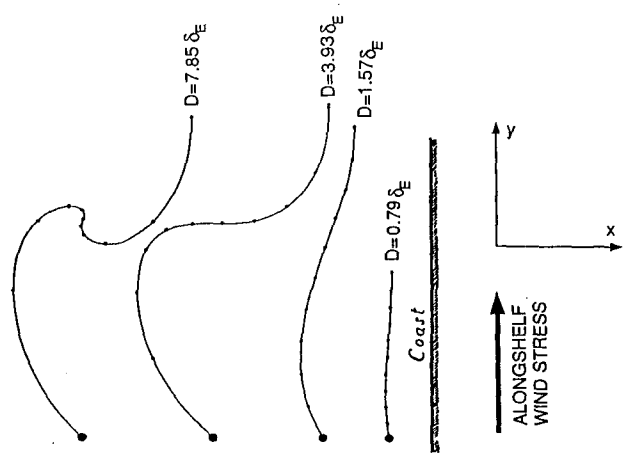

FIG. 1. Hodographs of the horizontal velocity in different water depths (D) for an alongshelf wind stress, from Ekman (1905). A vector from the large circle at the bottom of each hodograph to a point on the curve represents the current at some depth. The 10 small dots on each curve indicate the elevation above the bottom in $0.1D$ increments. Note the flow is alongshelf throughout the water column near the coast ($D = 0.79\delta_E$), but there are relatively large cross-shelf velocities near the bottom and surface in deeper water ($D = 7.85\delta_E$).

and

$$U = \int_{-D}^{0} u dz = 0 \quad \text{at} \quad x = 0, \qquad (4)$$

where $\boldsymbol{\tau}^S$ is the wind stress vector, z_{0S} and z_{0B} are surface and bottom roughnesses, and $D = D(x)$ is the water depth. For this two-dimensional model, the coastal boundary condition (4) and continuity imply that

$$U = 0 \quad \text{for all } x. \qquad (5)$$

The model is forced by the wind stress $\boldsymbol{\tau}^S$ and the alongshelf pressure gradient $\partial P/\partial y$. The cross-shelf pressure gradient $\partial P/\partial x$ is chosen to satisfy (5).

It is straightforward to include time dependence in the model and in the numerical scheme outlined below. For simplicity, however, only steady-state solutions are presented. Over typical inner shelf depths the model flow reaches steady state on time scales of about a day. Thus, the steady solutions are relevant to subinertial variability at midlatitudes.

b. Numerical scheme

Given the forcing terms $\boldsymbol{\tau}^S$ and $\partial P/\partial y$, the eddy viscosity profile $A_v(z)$ and $\partial P/\partial x$ at a particular cross-shelf location, (1), subject to (2) and (3), can be solved for $\mathbf{v}(z)$. While this system of equations can be solved analytically for certain choices of $A_v(z)$, to maintain flexibility in the choice of eddy viscosity profiles, a numerical scheme outlined in Patankar (1980) is used, with the vectors represented in complex notation. The procedure consists of a control volume representation in the vertical and involves solving a tridiagonal matrix.

The standard grid consists of 1001 points in the vertical with logarithmically increasing grid spacing extending from the surface and bottom boundaries. Increasing the number of grid points by a factor of 2 in several model runs gave almost identical results, indicating that the vertical structure is well resolved by the standard logarithmic grid.

Since many of the eddy viscosity profiles considered depend on the bottom stress, which is not known a priori, an iterative scheme is required (e.g., Madsen 1977). To begin the iteration, an initial guess of the bottom stress is made based on the depth-averaged alongshelf component of (1)

$$0 = -\frac{\partial P}{\partial y} + \frac{\tau^{Sy}}{D} - \frac{\tau^{By}}{D}, \qquad (6)$$

assuming $|\tau^B| \approx |\tau^{By}|$. This estimate of the bottom stress is used to determine the eddy viscosity profile and (1) is solved for $v(z)$. The resulting velocity profile is then used to estimate a new bottom stress that is in turn used to determine a new eddy viscosity profile. This procedure generally converges in a few iterations and is stopped when the change in the bottom shear velocity ($u_*^B = (|\tau^B/\rho_0|)^{1/2}$) is less than 10^{-4} m s^{-1}.

An iterative scheme is also used to find the value of $\partial P/\partial x$ that satisfies (5). An initial guess is made, again based on the depth-averaged form of (1), and the resulting velocity profile is used to estimate U. Subsequent estimates of $\partial P/\partial x$ are found using a linear search procedure to minimize U. In most cases a $\partial P/\partial x$ that yields an fU less than a few percent of the terms in (6) is achieved in 5–10 iterations. Jenter and Madsen (1989) use a similar procedure in their study of bottom stress for wind-driven depth-averaged flows. The numerical model was compared to analytic solutions for a constant eddy viscosity profile and for the bilinear eddy viscosity profile in deep water (Madsen 1977). In both cases the numerical model results agree with the analytic solutions to within one percent.

c. *Eddy viscosity profiles*

Five forms of the eddy viscosity profile were examined (Fig. 2): a constant eddy viscosity (Ekman 1905; Mitchum and Clarke 1986); a bilinear profile (Madsen 1977); a bilinear-cutoff profile (Deardorff 1972; Smith and Long 1976); a cubic profile (Signell et al. 1990); and a bilinear that decays exponentially toward zero in the interior (Long 1981; Glenn 1983). With the exception of the constant profile, all these eddy viscosity profiles have the form $A_v = \kappa u_* z'$ near the boundaries. They differ in how they extend into the interior of the fluid.

The bilinear profile suggested by Madsen (1977) and subsequently used in a number of applications (Jenter and Madsen 1989; Poon and Madsen 1991) extends the linear profiles into the interior. The vertical extent of the linear portions associated with the surface and bottom stresses are weighted by their respective u_*, so that the stronger stress influences more of the water column. This generally leads to a discontinuity in the eddy viscosity profile at the matching depth (Jenter and Madsen 1989).

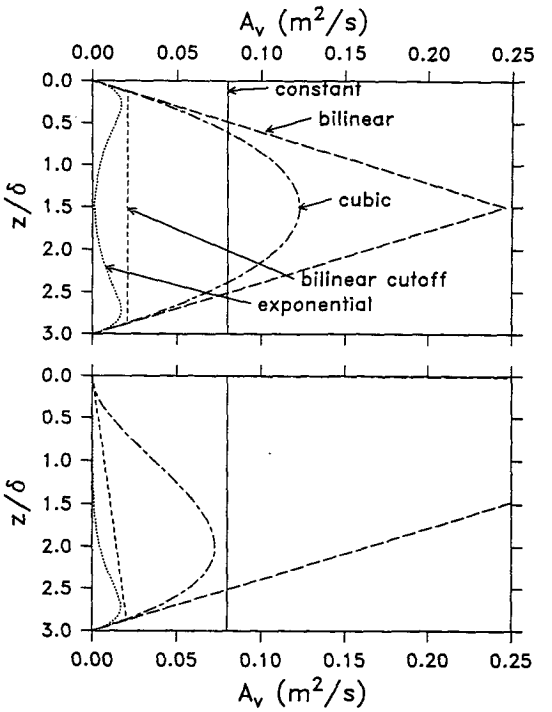

FIG. 2. Examples of the five eddy viscosity profiles examined in this study for the cases of a wind-driven flow (upper panel) and a pressure gradient driven flow (lower panel). The bilinear profile in the lower panel extends out to $A_v = 0.5$ (m^2 s^{-1}).

The cubic profile is the simplest polynomial that can match the two constraints at each boundary: that the eddy viscosity approach zero and the slope be κu_* (Signell et al. 1990), where u_* will in general be different at the surface and bottom boundaries. The cubic profile typically is similar to the bilinear profile though it has a smaller maximum in the interior and no discontinuity. In contrast to the bilinear profile, the weaker stress (surface or bottom) influences the larger fraction of the cubic profile.

The bilinear-cutoff profile is linear near the boundaries and constant in the interior. This is based on the notion that the eddy viscosity will not continue to grow indefinitely away from the boundary (e.g., Deardorff 1972). Typical choices for the distance from the boundary beyond which the eddy viscosity is constant are around 10% of the turbulent boundary layer scale δ (e.g., Smith and Long 1976) (where $\delta = \kappa u_*/f$). Ten percent is the choice used here. In the present application, since the surface and bottom boundary cutoff values for the eddy viscosity are not generally the same, they are joined by a linear interior profile. In very shallow water (less than 20% of the Ekman scale) the bilin-

ear-cutoff profile becomes identical to the bilinear profile.

The exponential profile is similar to the bilinear-cutoff profile except that away from the boundary the eddy viscosity decays exponentially toward zero; that is, $A_v(z') = \kappa u_* z' \exp(-z'/l)$ (Long 1981; Glenn 1983; Sanford 1984), where l is the exponential decay scale, which was somewhat arbitrarily chosen to be 0.27δ. For this choice the eddy viscosity decays to about 1% of its maximum value at a distance of 2δ from the boundary in deep water. This choice also yields a maximum eddy viscosity similar to the bilinear cutoff (Fig. 2). This eddy viscosity profile is qualitatively similar to the profiles from more sophisticated turbulence closure models (e.g., Weatherly and Martin 1978). The effect of varying the vertical scale of both the bilinear cutoff and exponential eddy viscosity profiles is examined in section 3.

3. Model comparisons

In this section the results of model runs using the five eddy viscosity profiles in Fig. 2 are compared. Two basic cases are considered: the response to an alongshelf wind stress and the response to an alongshelf pressure gradient.

a. Alongshelf wind stress

The model described in the previous section was run for each of the eddy viscosity profiles assuming a constant, spatially uniform, alongshelf wind stress and no alongshelf pressure gradient. Thus, based on the surface stress, the turbulent boundary layer scale δ and the deep-water Ekman transport $U_E = \tau/\rho_0 f$ were each constant. The vertically averaged alongshelf momentum balance (6) under these assumptions yields the simple result that the alongshelf component of the bottom stress equals the surface stress. Therefore, the cross-shelf Ekman transport in the bottom boundary layer will also equal U_E in deep water and assuming $|\tau^B| \approx |\tau^{By}|$, the bottom boundary layer scale will be approximately δ. The model inputs were $\tau^S = 1$ dyn cm^{-2}, $f = 10^{-4}$ s^{-1}, an effective roughness $z_0 = 0.01$ m at both the surface and bottom (e.g., Drake et al. 1992), and water depths ranging from 0.1 to 10 δ. These values give $\delta = 40$ m and $U_E = 1$ m^2 s^{-1}. The value of the constant eddy viscosity was chosen to give $\delta_E = (2A_v/f)^{1/2} = 40$ m. This results in an eddy viscosity of 0.08 m^2 s^{-1}, which is rather large but is appropriate for comparisons with the other profile results since the depth will be normalized by δ. As pointed out by Peggion and Weatherly (1991) the constant eddy viscosity may be chosen to match the bottom drag coefficient rather than the bottom boundary layer scale. This alternate choice is discussed below.

The normalized cross-shelf transport in the upper half of the water column, U_0/U_E, is plotted versus D/δ in Fig. 3 for the five eddy viscosity profiles. Here U_0 is estimated as the cross-shelf transport above the central zero crossing of the flow. Since the depth-integrated cross-shelf transport is zero by (5), the cross-shelf transport in the lower half of the water column must be equal in magnitude, but opposite in direction, to the cross-shelf transport in the upper water column. The cross-shelf structure of U_0/U_E falls into three main regions. For $D/\delta < 0.4$, rotation is unimportant and there is essentially no cross-shelf circulation. For $D/\delta > 4$, $U_0/U_E \sim 1$, which is the deep water solution. There is a 10%–20% overshoot ($U_0/U_E > 1$) in all the profiles. The overshoot has the largest cross-shelf extent for the cubic and bilinear profiles, for which U_0 exceeds U_E well beyond $D/\delta = 10$. This overshoot is a consequence of the reversal in the flow near the base of the Ekman layer associated with Ekman spiraling.

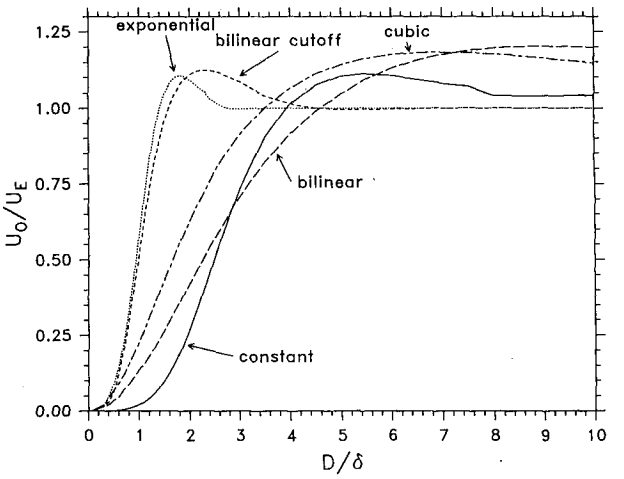

FIG. 3. The wind-driven cross-shelf transport in the upper water column U_0 normalized by the Ekman transport U_E plotted against the water depth D normalized by the turbulent Ekman scale δ for each of the five eddy viscosity profiles shown in Fig. 2. Since the net cross-shelf transport is zero, the upper and lower water column transports have equal magnitudes and opposite directions.

The most variation between the models occurs over the range $0.4 < D/\delta < 4$, the inner shelf where the cross-shelf divergence in the Ekman transport occurs. The divergence in the Ekman transport occurs in deeper water for the constant eddy viscosity model than for the other models. At $D/\delta = 1$ there is an order of magnitude difference in the cross-shelf transport between the bilinear cutoff and the constant eddy viscosity model. The two profiles with larger interior eddy viscosities (bilinear and cubic) diverge in deeper water and over a wider area than the two profiles with smaller interior eddy viscosities (bilinear cutoff and exponential). This is not surprising since the region where the divergence occurs depends on the extent to which there is a direct transfer of momentum from the surface to the bottom, which in turn will depend on the interior eddy viscosity. The exponential and bilinear-cutoff

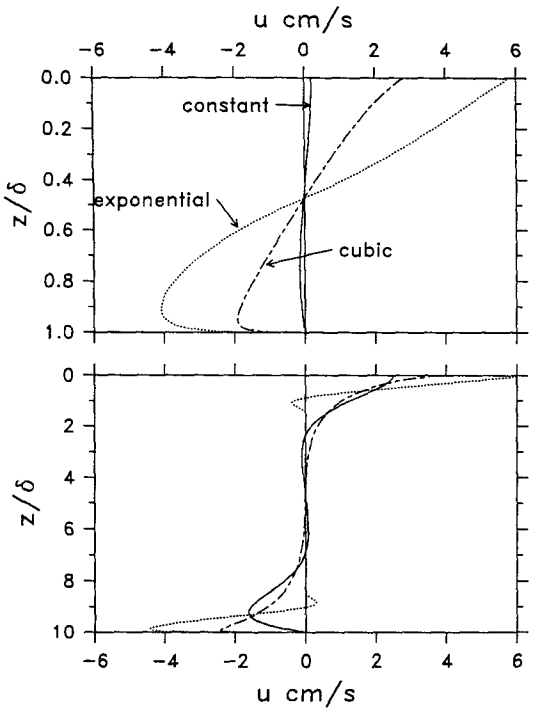

FIG. 4. Examples of the vertical profiles of cross-shelf velocity for three of the eddy viscosity profiles: (upper panel) the vertical profiles for $D/\delta = 1$ and (lower panel) the profiles for $D/\delta = 10$. The current profiles for the bilinear eddy viscosity profile (not shown) resemble those for the cubic eddy viscosity profile and the current profiles for the bilinear cutoff resemble those for the exponential eddy viscosity profile.

models diverge in the shallowest water because their effective boundary layer scale is actually about half δ. This is clear in vertical profiles of the cross-shelf velocity (Fig. 4) and is easily understood. The bilinear-cutoff eddy viscosity is roughly constant and equal to $A_{vc} = \kappa u_*(0.1\delta)$ over the outer 90% of the boundary layer, where rotation is important. Using this eddy viscosity to estimate the effective boundary layer scale yields $\delta_{blc} = (2A_{vc}/f)^{1/2} = 0.45\delta$. A similar argument holds for the exponential profile with the maximum eddy viscosity determining the boundary layer scale.

A primary consequence of the cross-shelf divergence of the Ekman transport is that it drives a vertical velocity (i.e., upwelling or downwelling). The offshore location and width of the cross-shelf divergence determines where the upwelling or downwelling occurs and how strong it is. The vertical velocity at midwater column can be estimated by integrating the continuity equation from the surface to the central zero crossing of the cross-shelf velocity, which yields

$$w(z \approx -D/2) = \frac{\partial U_0}{\partial x} = \frac{\partial U_0}{\partial D}\frac{\partial D}{\partial x}. \qquad (7)$$

Assuming a bottom slope of 10^{-3} and estimating $\partial U_0/\partial D$ from Fig. 3, estimates of the vertical velocity from (7) are shown in Fig. 5. Note that the cross-shelf scales in Fig. 5 seem unreasonably large. In most cases stratification will limit the thickness of the boundary layers over the mid and outer shelf (e.g., Lentz and Trowbridge 1991; Lentz 1992) and hence the cross-shelf extent of the inner-shelf region. Consequently, these figures are intended to indicate tendencies and not realistic cross-shelf structure. From (7), the magnitude of the vertical velocity is proportional to the bottom slope. Continuity requires that the total vertical transport equal the offshore (or onshore) transport in deep water, that is, the Ekman transport. Consequently, since the magnitude of the vertical velocity is proportional to the bottom slope, the cross-shelf scale of the vertical velocity must be inversely proportional to the bottom slope; that is, the gentler the bottom slope the broader the region over which the cross-shelf divergence in the Ekman transport occurs. The profiles with the weakest interior eddy viscosities have the largest vertical velocities over the narrowest region in the shallowest water. Figures 3 and 5 summarize the primary result of this study. The cross-shelf structure of the cross-shelf circulation over the inner shelf, and hence the location and width of the cross-shelf divergence in the Ekman transport, are sensitive to the form of the eddy viscosity profile. This suggests that any model of the inner shelf that seeks to determine the cross-shelf circulation due to wind forcing must accurately represent the vertical structure of the mixing.

In contrast to the cross-shelf flow, the alongshelf flow is not very sensitive to the form of the eddy viscosity profile (Figs. 6 and 7), with the exception of the constant eddy viscosity. The two profiles with small interior eddy viscosities have slightly larger alongshelf velocities than the profiles with large interior eddy viscosities. This is a manifestation of the influence of the eddy

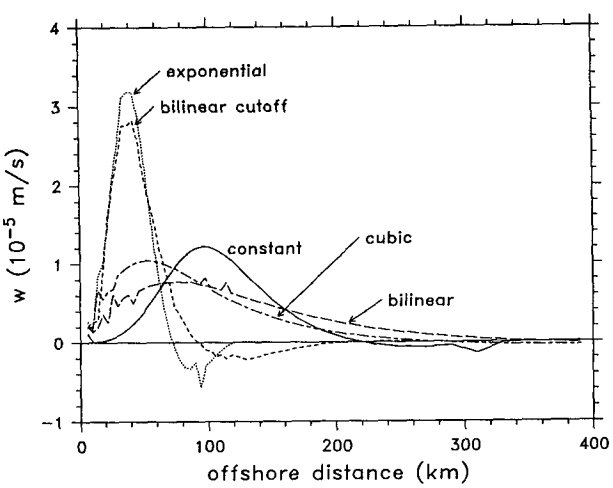

FIG. 5. Estimates of the vertical velocity at mid-water column as a function of offshore distance for the five eddy viscosity profiles. The vertical velocities were estimated from (7) assuming a bottom slope of 10^{-3}.

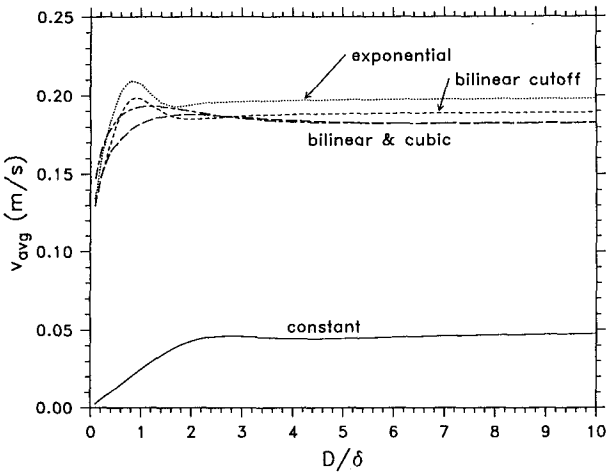

FIG. 6. The wind-driven depth-averaged alongshelf velocity plotted against D/δ for each of the five eddy viscosity profiles shown in Fig. 2.

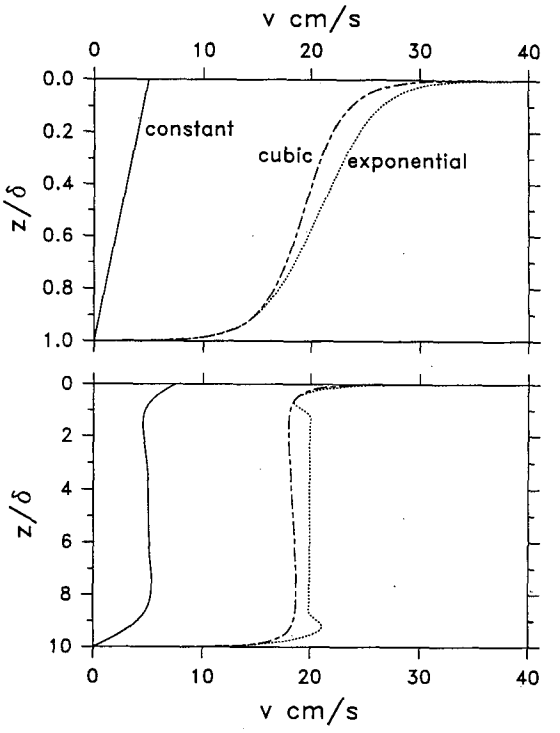

FIG. 7. Examples of the vertical profiles of alongshelf velocity for three of the eddy viscosity profiles. The upper panel shows the vertical profiles for $D/\delta = 1$, while the lower panel shows the profiles for $D/\delta = 10$.

viscosity in the outer portion of the boundary layer on the relationship between the depth-averaged velocity and the bottom stress. The constant eddy viscosity profile gives a much weaker depth-averaged alongshelf flow, because the constant eddy viscosity extends all the way to the bottom and consequently the boundary is less slippery than for the profiles where the eddy viscosity goes linearly to zero at the boundary. A smaller constant eddy viscosity ($A_v = 0.005$ m^2 s^{-1}) yields the same depth-averaged alongshelf velocity in deep water as the other models (i.e., the same bottom drag coefficient) (Peggion and Weatherly 1991), but the corresponding δ_E is smaller than for the other models. The resulting dependence of U_0/U_E on D/δ_E is identical to that shown in Fig. 3, when the smaller δ_E is used to normalize D.

Observations of shelf flows are commonly from moorings at a fixed water depth. Since δ depends on the wind stress, the width of the inner shelf will vary with the wind stress. Consequently, a fixed mooring site may be in or out of the inner shelf as the wind stress varies. This can be seen in Fig. 8, which shows the cross-shelf transport as a function of the wind stress at a particular isobath ($D = 40$ m) for the five eddy viscosity profiles. There are notable differences in the onshore transport response to alongshelf wind stress for the various eddy viscosity profiles. For small wind stresses, $\tau^{Sy}/\rho_0 < 0.2 \times 10^{-4}$ (m s^{-1})^2, all the profiles tend toward the deep-water linear relationship that the onshore transport equals the deep water Ekman transport. However, for larger wind stresses, the onshore transport response reaches a maximum and then actually declines for the profiles with small interior eddy viscosities. This peak in the onshore response occurs near $D = \delta$ [i.e., when $\tau^{Sy}/\rho_0 = 10^{-4}$ (m s^{-1})^2 for the parameters used]. For the profiles with large interior eddy viscosities (cubic and bilinear), the onshore transport is nearly constant for $\tau^{Sy}/\rho_0 > 0.5 \times 10^{-4}$ (m s^{-1})^2. This indicates that for a given location under variable wind conditions the relationship between the on/offshore transport and the wind stress will be sensitive to the form of the eddy viscosity profile. This

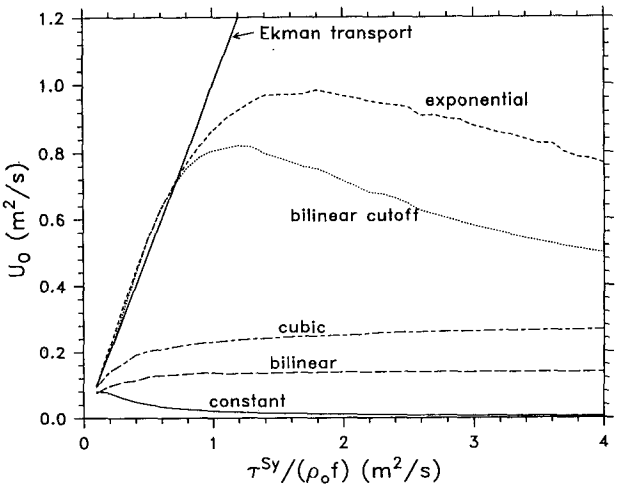

FIG. 8. The cross-shelf transport U_0 versus $\tau^{Sy}/(\rho_0 f)$ in 40 m of water for the five eddy viscosity profiles.

suggests that for inner-shelf regions where the wind stress is the dominant forcing a scatterplot of on/offshore transport versus wind stress may suggest the qualitative form of the eddy viscosity profile. As expected from the results shown in Fig. 6, the depth-averaged alongshelf velocity response to the alongshelf wind stress at a given location is essentially the same for all the eddy viscosity profiles except the constant eddy viscosity.

For the eddy viscosity profiles examined, two or three parameters must be specified besides the forcing, the water depth, and the latitude (i.e., Coriolis parameter). With the exception of the constant eddy viscosity case, surface and bottom roughnesses, z_{0S} and z_{0B}, must be prescribed. Additionally, a vertical scale must be specified for the bilinear cutoff and exponential profiles. The sensitivity of the model results to these parameters is discussed here. One might anticipate that the cross-shelf transports would be insensitive to the surface and bottom roughnesses, since the cross-shelf transports depend on the surface and bottom stresses, which are independent of the roughnesses (6). This is confirmed in Fig. 9 (upper panel), which shows U_0/U_E as a function of D/δ for z_{0B} = 0.001, 0.01, and 0.1 m. For a two order of magnitude change in z_{0B} there is almost no change in U_0/U_E. The particular example shown is for the bilinear eddy viscosity profile, but the results are the same for the other forms of the eddy viscosity profile that depend on z_{0B}. The depth-averaged alongshelf velocity should be sensitive to z_{0B}, or more precisely to $\log(z_{0B})$, because z_{0B} influences the relationship between the bottom stress and the interior alongshelf velocity by changing the bottom drag coefficient. Again the results in Fig. 9 (lower panel) confirm this hypothesis. The solutions are not very sensitive to the value of the surface roughness z_{0S} because the surface stress is prescribed.

The cross-shelf transports for the bilinear cutoff and exponential eddy viscosity profiles are sensitive to the choice of the vertical scale needed to specify the profiles. This is obvious given the argument above that the effective boundary layer scale depends on the maximum eddy viscosity within the boundary layer. Thus, a shorter vertical scale, which results in a smaller maximum eddy viscosity within the boundary layer, would cause the Ekman transport divergence to occur in shallower water, whereas a larger vertical scale causes the transport divergence to occur in deeper water (Fig. 10). The vertical scale for the bilinear cutoff and exponential profiles also influences the alongshelf flow with slightly larger alongshelf velocities corresponding to smaller scales, that is, weaker maximum eddy viscosities.

b. *Alongshelf pressure gradient*

The response to an alongshelf pressure gradient is examined briefly here because it differs from the wind-driven response in a number of ways. Assuming the

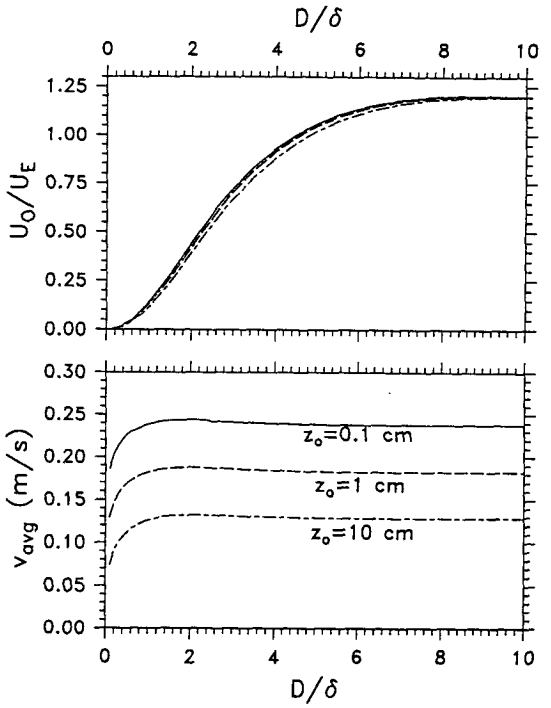

FIG. 9. The normalized cross-shelf transport U_0/U_E (upper panel) and depth-averaged alongshelf velocity v_{avg} (lower panel) vs D/δ for different values of the bottom roughness z_{0B}. The bilinear eddy viscosity profile is used in this example but the results are similar for the other eddy viscosity profiles.

surface stress is zero, the boundary layer scale δ and the deep-water Ekman transport U_E are both determined by the bottom stress. However, if $\partial P/\partial y$ is uniform across the shelf, (6) indicates that the bottom stress must increase as the water depth increases (given $\tau^{Sy} = 0$). Therefore,

$$U_E = \frac{\tau^{By}}{\rho_0 f} = \frac{1}{\rho_0}\frac{\partial P}{\partial y}\frac{D}{f}, \tag{8}$$

and

$$\delta \approx \frac{\kappa}{f}\left(\frac{D}{\rho_0}\left|\frac{\partial P}{\partial y}\right|\right)^{1/2}, \tag{9}$$

assuming $\tau^{By} \gg \tau^{Bx}$, so $u_* \approx (|\tau^{By}|/\rho_0)^{1/2}$. From (8) there will be a cross-shelf divergence in U_E proportional to $\partial D/\partial x$, even in water deep compared to δ.

To facilitate comparisons of the response to an alongshelf pressure gradient with the wind-driven response, the cross-shelf transport was normalized by U_E and the depth was normalized by δ as for the wind stress. This may be viewed as the response to an alongshelf pressure gradient that varies across the shelf so that the bottom stress is constant. Even in this case there is a marked difference in the cross-shelf structure of U_0/U_E (Fig. 11). As for the wind-driven case there are three regions. For $D/\delta < 0.4$, rotation is unimpor-

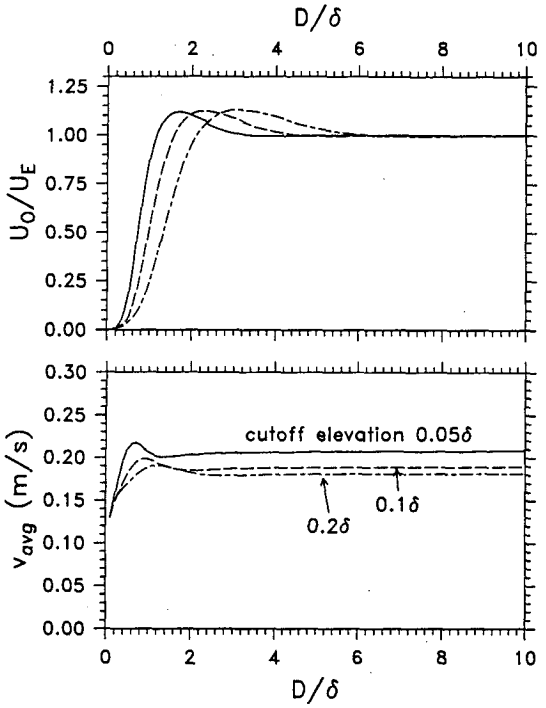

FIG. 10. The normalized cross-shelf transport U_0/U_E (upper panel) and depth-averaged alongshelf velocity (lower panel), vs D/δ for different values of the vertical cutoff scale for the bilinear eddy viscosity profile. Results for the exponential eddy viscosity profile are similar.

tant and the cross-shelf circulation is very weak. Most of the divergence in the Ekman transport still occurs over the inner-shelf region $0.4 < D/\delta < 4$, and this is the region where the response is most sensitive to the form of the eddy viscosity profile. The differences in the cross-shelf circulation in this region for the various forms of the eddy viscosity profile are qualitatively the same as for the wind-driven case.

The most notable difference from the wind-driven response occurs for $D/\delta > 4$, where the curves in Fig. 11 approach the asymptote $U_0/U_E = 1$ more slowly and there is no overshoot. This response may be understood by considering the cross-shelf circulation (Fig. 12). There is an onshore flow in the bottom boundary layer and a vertically uniform geostrophic offshore flow in the interior. Integrating the alongshelf component of (1) from the bottom to the top of the boundary layer ($h_{BL} = 2\delta$ for the constant, bilinear and cubic profiles, and $h_{BL} = \delta$ for the bilinear cutoff and exponential profiles) yields

$$U_B \approx \frac{1}{\rho_0}\frac{\partial P}{\partial y}\frac{h_{BL}}{f} - \frac{\tau^{By}}{\rho_0 f} = -\frac{\tau^{By}}{\rho_0 f}(1 - h_{BL}/D), \quad (10)$$

where

$$U_B = \int_{-D}^{-D+h_{BL}} u\, dz,$$

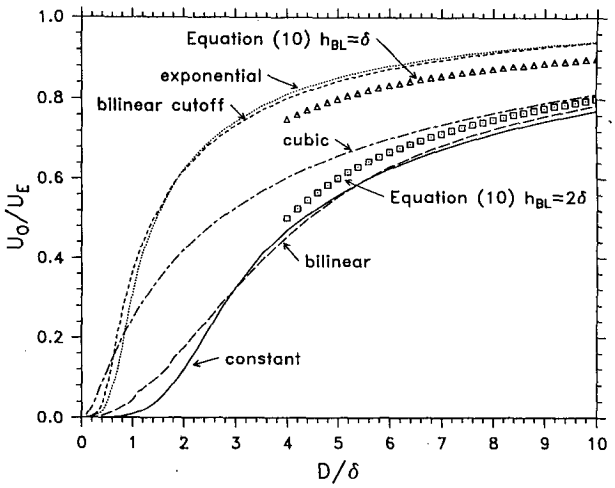

FIG. 11. Same as Fig. 3 but for a flow driven by an alongshelf pressure gradient rather than a wind stress. The symbols show estimates based on (10) for $4 < D/\delta < 10$.

and (6) has been used to relate $\partial P/\partial y$ and τ^{By}, assuming $\tau^{Sy} = 0$. The net onshore (or offshore transport) equals the deep water Ekman transport ($\tau^{By}/\rho_0 f$) minus the portion of the geostrophic interior transport that occurs within the bottom boundary layer. Thus the onshore transport should approach the asymptote U_E for large D/δ. Predictions based on (10) represent the model dependencies for $D/\delta > 4$ fairly well (Fig. 11). The underestimate of the responses for the bilinear cutoff and exponential eddy viscosity profiles using $h_{BL} = 2\delta$ occurs because using the central zero crossing results in an overestimate of U_0 due to the boundary layer response that occurs above the central zero crossing (Fig. 12). The alongshelf velocity response (not

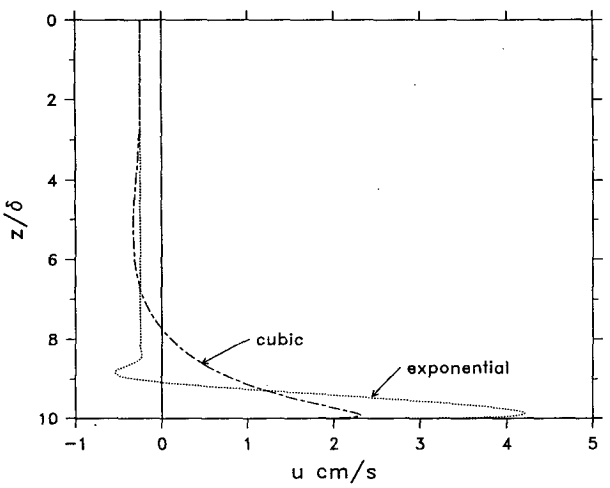

FIG. 12. Cross-shelf current profiles driven by an alongshelf pressure gradient in deep water ($D/\delta = 10$) for the cubic and exponential eddy viscosity profiles.

shown) is essentially the same as for the wind stress (Fig. 6).

4. Discussion and summary

The model results presented suggest that the characteristics of the alongshelf flow over the inner shelf are relatively insensitive to the form of the eddy viscosity profile except for the constant eddy viscosity, while some aspects of the cross-shelf circulation are sensitive to the form of the eddy viscosity profile. In particular, the location and width of the region of cross-shelf divergence in the Ekman transport is sensitive to the form of the eddy viscosity profile. Profiles with relatively weak interior eddy viscosities have narrower regions of cross-shelf divergence in shallower water than profiles with larger interior eddy viscosities. The sensitivity of the cross-shelf divergence in the Ekman transport to the form of the eddy viscosity profile is not surprising. In deep water the presence of a spatially uniform surface stress can only be transmitted to the interior and to the bottom boundary layer through the coastal boundary condition since the wind-driven stress is confined by rotation to the surface Ekman layer. Thus the path of communication between the surface boundary layer and the interior or bottom boundary layer is across shelf. The same argument holds for communication between the interior and bottom boundary layer for an alongshelf pressure gradient–driven flow. In contrast, in very shallow water the stress is transmitted directly from the surface to the bottom. Thus the cross-shelf divergence in the Ekman transport begins to occur where there is sufficient interior stress to transfer momentum directly through the water column, circumventing the cross-shelf circulation pathway. Where this occurs will depend on the strength of turbulent mixing in the interior.

This study suggests that caution must be used in generalizing model results for the inner shelf based on a particular form of the turbulent mixing. Given the evidence that a constant eddy viscosity is not realistic near the boundaries (e.g., Weatherly 1972), this form of the eddy viscosity profile should not be used in studies focusing on problems dependent on or related to the inner-shelf cross-shelf circulation. However, there is little observational evidence at present to suggest that any one of the other four eddy viscosity profiles is more realistic than the others.

Lentz (1994) used a time-dependent version of the model described in section 2 to simulate observations from a mooring on the northern California inner shelf where the stratification was weak and observed currents were driven by a combination of wind stress and alongshelf pressure gradient forcing. Simulations were made using four different forms for the eddy viscosity profile: the bilinear, cubic, bilinear cutoff, and exponential (Fig. 2). All four eddy viscosity profiles yielded similar results and good agreement with the observations, indicating that the basic features of the flow were not very sensitive to the form of the eddy viscosity profile. This was primarily because the dominant characteristics of the flow were associated with the alongshelf current. The cubic eddy viscosity profile yielded a slightly better representation of the magnitude and vertical structure of the relatively weak cross-shelf current than the other eddy viscosity profiles. While Lentz's (1994) comparisons suggest that a simple eddy viscosity model can account for most of the observed variance in the northern California observations he examined, the comparison was not definitive in identifying one form of the eddy viscosity profile as more appropriate for the northern California shelf observations.

At present, relatively little is known about turbulence over the inner shelf. Obviously, the presence or absence of stratification will strongly modify the characteristics of the turbulence. Consequently, the vertical structure of the turbulence is likely to vary across the shelf, if the inner shelf is unstratified and the middle and outer shelf are stratified. Even in the absence of stratification other factors may influence the vertical structure of the turbulence. For example, the presence or absence of strong tidal energy may influence the form of the turbulent mixing profile (e.g., Davies and Jones 1990). For the northern California shelf, Lentz (1994) hypothesized that large rock outcrops significantly increased the bottom drag on the flow. Such topographic features may also alter the vertical structure of the turbulence. It seems likely that surface gravity waves may also be a significant influence on the turbulence in shallow water. The model results presented here suggest that the vertical structure of turbulent mixing is a key element of the inner-shelf dynamics and its role in the overall shelf circulation. While application of simple models in combination with current observations (Lentz 1994) may provide indirect insight into the characteristics of turbulence over the inner shelf, field studies aimed at determining the characteristics of turbulence over inner shelves are clearly needed.

Acknowledgments. I appreciate thoughtful comments on this study from J. Trowbridge, K. Brink, G. Gawarkiewicz, D. Chapman, and R. Beardsley (all at Woods Hole Oceanographic Institution). This work was funded by the Ocean Sciences Division of the National Science Foundation under Grant OCE-9115713 and by the Office of Naval Research Coastal Science Program under Grant N00014-89-J-1074.

REFERENCES

Agrawal, Y. C., E. A. Terray, M. A. Donelan, P. A. Hwang, A. J. Williams, W. M. Drennan, K. K. Kahma, and S. A. Kitaigorodskii, 1992: Enhanced dissipation of kinetic energy beneath surface waves. *Nature*, **359**, 219–220.

Allen, J. S., R. C. Beardsley, J. O. Blanton, W. C. Boicourt, B. Butman, L. K. Coachman, A. Huyer, T. H. Kinder, T. C. Royer, J. D. Schumacher, R. L. Smith, and W. Strurges, 1983: Physical

oceanography of continental shelves. *Rev. Geophys. Space Phys.*, **21**(5), 1149–1181.

Davies, A. M., and J. E. Jones, 1990: Application of a three-dimensional turbulence energy model to the determination of tidal currents on the northwest European shelf. *J. Geophys. Res.*, **95**(C10), 18 143–18 162.

Deardorff, J. W., 1972: Numerical investigation of neutral and unstable planetary boundary layers. *J. Atmos. Sci.*, **29**, 91–115.

Drake, D. E., D. A. Cacchione, and W. D. Grant, 1992: Shear stress and bed roughness estimates for combined wave and current flows over a rippled bed. *J. Geophys. Res.*, **97**(C2), 2319–2326.

Ekman, V. W., 1905: On the influence of the earth's rotation on ocean currents. *Ark. Mat. Aston. Fys.*, 2(11), 1–53.

Gill, A. E., and A. J. Clarke, 1974: Wind-induced upwelling, coastal currents and sea-level changes. *Deep-Sea Res.*, **21**, 325–345.

Glenn, S. M., 1983: A continental shelf bottom boundary layer model: The effects of waves, currents and moveable bed. Ph.D. thesis, Woods Hole Oceanographic Institute, Massachusetts Institute of Technology, 237 pp.

Grant, W. D., and O. S. Madsen, 1986: The continental-shelf bottom boundary layer. *Ann. Rev. Fluid Mech.*, **18**, 265–305.

Jenter, H. L., and O. S. Madsen, 1989: Bottom stress in wind-driven depth-averaged coastal flow. *J. Phys. Oceanogr.*, **19**(7), 962–974.

Lee, T. N., E. Williams, R. Evans, J. Wang, and L. Atkinson, 1989: Response of South Carolina continental shelf waters to wind and gulf stream forcing during winter of 1986: *J. Geophys. Res.*, **94**(C8), 10 715–10 754.

Lentz, S. J., 1992: The surface boundary layer in coastal upwelling regions. *J. Phys. Oceanogr.*, **22**(12), 1517–1539.

——, 1994: Current dynamics over the northern California inner shelf. *J. Phys. Oceanogr.*, **24**, 2461–2478.

——, and J. H. Trowbridge, 1991: The bottom boundary layer over the northern California shelf. *J. Phys. Oceanogr.*, **21**(8), 1186–1201.

Long, C. E., 1981: A simple model for time-dependent stably stratified turbulent boundary layers. Tech. Rep. Special Report No. 95, University of Washington, Seattle, Washington, 170 pp.

Madsen, O. S., 1977: A realistic model of the wind-induced Ekman boundary layer. *J. Phys. Oceanogr.*, **7**, 248–255.

Mitchum, G. T., and A. J. Clarke, 1986: The frictional nearshore response to forcing by synoptic scale winds. *J. Phys. Oceanogr.*, **16**, 934–946.

Patankar, S. V., 1980: *Numerical Heat Transfer and Fluid Flow.* Hemisphere Publishing, 197 pp.

Peggion, G., and G. L. Weatherly, 1991: On the interaction of the bottom boundary layer and deep rings. *Mar. Geol.*, **99**(3/4), 329–342.

Poon, Y. K., and O. S. Madsen, 1991: A two-layer wind-driven coastal circulation model. *J. Geophys. Res.*, **96**(C2), 2535–2548.

Richman, J. G., R. A. de Szoeke, and R. E. Davis, 1987: Measurements of near-surface shear in the ocean. *J. Geophys. Res.*, **92**(C3), 2851–2858.

Sanford, L. P., 1984: The interaction of high frequency internal waves and bottom boundary layers on the continental shelf. Ph.D. thesis, Woods Hole Oceanographic Institution, Massachusetts Institute of Technology, 232 pp.

Signell, R. P., R. C. Beardsley, H. C. Graber, and A. Capotondi, 1990: Effect of wave–current interaction on wind-driven circulation in narrow, shallow embayments. *J. Geophys. Res.*, **95**(C6), 9671–9678.

Smith, J. D., and C. E. Long, 1976: The effect of turning in the bottom boundary layer on continental shelf sediment transport. *Mem. Soc. Roy. Sci. Liege, Ser. 6*, **X**, 369–396.

Thomas, J. H., 1975: A theory of steady wind-driven currents in shallow water with variable eddy viscosity. *J. Phys. Oceanogr.*, **5**, 136–142.

Weatherly, G. L., 1972: A study of the bottom boundary layer of the Florida Current. *J. Phys. Oceanogr.*, **2**, 54–72.

——, and P. J. Martin, 1978: On the structure and dynamics of the oceanic bottom boundary layer. *J. Phys. Oceanogr.*, **8**, 557–570.

Witten, A. J., and J. H. Thomas, 1976: Steady wind-driven currents in a large lake with depth-dependent eddy viscosity. *J. Phys. Oceanogr.*, **6**(1), 85–92.